Inorg. Chem. **2004**, *43*, 663–673

Intense Fluorescence of Metal-to-Ligand Charge Transfer in [Pt(0)(binap)$_2$] [binap = 2,2′-Bis(diphenylphosphino)-1,1′-binaphthyl]

Zainul Abedin-Siddique, Takeshi Ohno, and Koichi Nozaki*

Department of Chemistry, Graduate School of Science, Osaka University, 1-16 Machikaneyama, Toyonaka, Osaka 560-0043, Japan,

Taro Tsubomura

Department of Applied Chemistry, Seikei University, Kichijoji-Kitamachi, Musashino, Tokyo 180-8633, Japan

Received May 16, 2003

[Pt(0)(binap)$_2$] (binap = 2,2′-bis(diphenylphosphino)-1,1′-binaphthyl) is found to exhibit a luminescence from metal-to-ligand charge transfer state (MLCT) with a quantum yield of 0.12 and a lifetime of 1.2 μs in toluene at an ambient temperature. Prompt fluorescence with a quantum yield of 1.6×10^{-4} is observed by means of a picosecond time-correlated single photon counting technique. The spectrum of the steady-state luminescence is almost identical to that of the prompt fluorescence, indicating that the intense luminescence is mainly delayed fluorescence from thermally activated ^{1}MLCT. The analysis of the temperature-dependent emission indicates that the energy difference between the ^{1}MLCT and ^{3}MLCT is 1.15×10^3 cm^{-1}. The lifetime of the prompt fluorescence is determined to be 3.2 ps from the decay of stimulated emission overlapped on subpicosecond transient absorption spectra. The lifetime of the ^{1}MLCT is much longer than expected from the large spin–orbit coupling constant of 5d (Pt) electrons (4000 cm^{-1}). Theoretical analysis based on density functional theory reveals that structural distortion in the MLCT states causes large energy splitting between HOMO and HOMO − 1, which prevents a very fast ISC induced by strong spin–orbit interactions between these orbitals. The relatively slow ISC is therefore induced by weak spin–orbit interactions (ca. 50 cm^{-1}) between ligand-centered molecular orbitals. Theoretical calculations indicate that the phosphorescence observed at lower temperatures is due to intensity borrowing from $4^1B_2 \rightarrow$ GS transition. However, the large energy difference between HOMO and HOMO − 2 reduces the extent of mixing between the lowest ^{3}MLCT and 4^1B_2 due to spin–orbit interaction, thereby decreasing the radiative rate of the phosphorescence.

Introduction

Photophysical studies of singlet metal-to-ligand charge transfer states (^{1}MLCT) have been a challenging topic in recent photochemistry of transition metal compounds since the electron injection from ^{1}MLCT of a ruthenium compound to TiO_2 film was found to be the primary process in a dye-sensitized solar cell.[1,2] In most transition metal compounds, the fluorescence from MLCT is not observed because a fairly strong spin−orbit coupling of d-electrons tends to induce very rapid intersystem crossing (ISC) ($>10^{13}$ s^{-1}). The recent development of ultrashort laser pulse technology has, however, allowed us to observe very short-lived fluorescence states. The lifetime of ^{1}MLCT for [Ru(bpy)$_3$]$^{2+}$, where bpy = 2,2′-bipyridine, one of the most widely studied d^6 metal compounds, was measured as 40 ± 15 fs using femtosecond fluorescence up-conversion spectroscopy, and the quantum yield of fluorescence (^{1}MLCT) was estimated to be less than 10^{-6}.[3] The ^{1}MLCT fluorescence of [Ru(II)(bpy)$_2$(dcbpy)]

* To whom correspondence should be addressed. E-mail: nozaki@ch.wani.osaka-u.ac.jp.

(1) (a) Hannappel, T.; Burfeindt, B.; Storck, W.; Willig, F. *J. Phys. Chem. B* **1997**, *101*, 6799. (b) Tachibana, Y.; Haque, S. A.; Mercer, I. P.; Durrant, J. R.; Klug, D. R. *J. Phys. Chem. B* **2000**, *104*, 1198. (c) Benko, G.; Kallioinen, J.; Korppi-Tommola, J. E. I.; Yartsev, A. P.; Sundstrom, V. *J. Am. Chem. Soc.* **2002**, *124*, 489.

(2) Iwai, S.; Hara, K.; Murata, S.; Katoh, R.; Sugihara, H.; Arakawa, H. *J. Chem. Phys.* **2000**, *113*, 366.

(3) Bhasikuttan, A. C.; Suzuki, M.; Nakashima, S.; Okada, T. *J. Am. Chem. Soc.* **2002**, *124*, 8398.

10.1021/ic034527z CCC: $27.50
Published on Web 12/16/2003

(dcbpy = 4,4′-dicarboxy-2,2′-bipyridine) adsorbed on a SnO_2 nanocrystal was detected as a stimulated emission by femtosecond pump−probe spectroscopy.[2] Kwok et al. found weak and broad MLCT fluorescence spectra in the measurement of resonance Raman spectra of [Pt(0)(dppm)(PhC≡C)$_2$] [dppm = bis(diphenylphosphino)methane], of which the yield and the lifetime were inferred to be ca. 10^{-6} and 80−130 fs, respectively.[4]

Some coordination compounds have been reported to exhibit fluorescence from thermally accessible ^{1}MLCT, namely delayed fluorescence. One typical example is [Cr(III)(urea)$_6$]$^{3+}$, showing broad fluorescence ($^4T_2 \rightarrow {}^4A_2$), in which $^4T_2$ was below the ^{2}E energy level or thermally accessible.[5] A Pt(II) compound with a terpyridine ligand having a pyrenyl moiety, [Pt(II)(4′-(1-pyrenyl)-2, 2′:6′,2″-terpyridine)Cl]$^+$, involved at least two different emitting excited states: a singlet [$^1\pi\pi^*$/^{1}ILCT] state with a radiative rate constant of ca. 10^6 s^{-1} and a triplet state with a rate of $\sim 10^2$ s^{-1}.[6] The short-lived fluorescence of this Pt(II) compound may come from a ligand-centered excited state which is not subject to the large spin−orbit coupling of the 5d electron.

In the previous study,[7] we found that the lowest ^{1}MLCT states in copper(I) bis(diimine) compounds, e.g., [Cu(I)(dmp)$_2$]$^+$ (dmp = 2,9-dimethyl-1,0-phenanthlorine), have a relatively long lifetime of around 15 ps though the spin−orbit coupling of the 3d-electron in copper(I) is as strong as that of 4d-electron in ruthenium(II).[8] The sluggishness of ISC was ascribed to structural distortion due to the Jahn−Teller effect in its MLCT excited state. The distortion from the tetrahedral structure caused energy splitting ($> 6.8 \times 10^3$ cm^{-1}) between HOMO and HOMO − 1 with large d-orbital contributions. As a result, the ISC process induced by a strong spin−orbit interaction between HOMO and HOMO − 1 was energetically unfavorable. The large energy splitting also reduces mixing due to the spin−orbit interaction between ^{1}MLCT and the lowest ^{3}MLCT, thereby yielding a low radiative phosphorescence rate (ca. 10^3 s^{-1}).[7] The idea that such peculiar photophysical features observed for the copper(I) compounds may be intrinsic to MLCT of d^{10} metal compounds with tetrahedral structure has prompted us to extend our study to other d^{10} metal compounds.

Phosphine and phosphite complexes of nickel(0), palladium(0), and platinum(0) (d^{10} metal compounds) have been reported to exhibit long-lived ($\sim\mu$s lifetime) emission at room temperature in fluid solution[9] and in the solid state,[10] which originated from the metal-centered ^{3}(d → p) state.[9] The lowest emissive excited states of tetrahedral compounds, [M(dppp)$_2$] (M = palladium and platinum, dppp = bis(diphenylphosphino)propane), were assigned to ^{3}(d → p) state.[11]

Tsubomura et al. have reported that one of the platinum(0) compounds, [Pt(binap)$_2$], exhibited intense red luminescence originating from an MLCT state in benzene.[12,13] The ligand, binap [binap = 2,2′-bis(diphenylphosphino)-1,1′-binaphthyl], with an extended π-electron system has a low energy π^*-acceptor orbital which is suitable for MLCT transition in the visible region.[14]

In this study, we focused on the dynamics and photophysical properties of MLCT in [Pt(0)(binap)$_2$]. Prompt

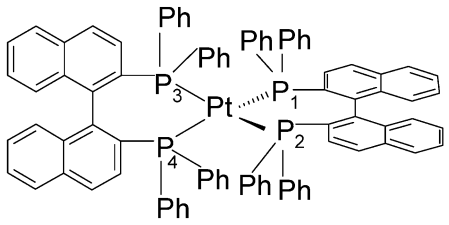

[Pt(binap)$_2$] (Ph=C$_6$H$_5$)

fluorescence was observed by means of a time-correlated single photon counting (TCSPC) technique and also by subpicosecond transient absorption spectroscopy. Intense emission at an ambient temperature was assigned to delayed fluorescence. To the best of our knowledge, this compound is the first example of the highest quantum yields of both prompt fluorescence (1.6×10^{-4}) and delayed fluorescence (0.11) from MLCT. The rate of intersystem crossing and the photophysical properties of the platinum(0) compound were analyzed on the basis of quantum chemical calculations and compared with those of copper(I)bis(diimine) compounds.

Experimental Section

(I) Materials. The solutions of ca. 10^{-5} M of [Pt(binap)$_2$][12] were deoxygenated by repeating freeze−pump−thaw cycles in a lab-made Pyrex vessel, and then, the solutions were transferred into an optical cell (1 mm × 10 mm). When the concentration was higher than 10^{-4} M, the concentration quenching of excited states was observed. The [Pt(binap)$_2$] solutions were photochemically unstable in air: the air-saturated deep red solutions of dichloromethane (CH_2Cl_2) or acetonitrile gradually paled during light irradiation. Even air-free solutions of CH_2Cl_2 were stable for several hours but gradually decomposed (~10% for 10 h) while a toluene solution was stable for several months. For emission measurements, the fluorescence-analysis grade benzene, CH_2Cl_2, acetonitrile, and

(4) Kwok, W. M.; Phillips, D. L.; Yeung, P. K.; Yam, V. W. W. *J. Phys. Chem. A* **1997**, *101*, 9286.
(5) (a) Porter, G. B.; Schlafer, H. L. *Z. Phys. Chem.* **1963**, *37*, 109. (b) Balzani, V.; Carassiti, V. *Photochemistry of coordination compounds*; Academic Press Inc.: London, 1970; p 107.
(6) Michalec, J. F.; Bejune, S. A.; Cuttell, D. G.; Summerton, G. C.; Gertenbach Field, J. S.; Haines, R. J.; McMillin, D. R. *Inorg. Chem.* **2001**, *40*, 2193
(7) Siddique, Z. A.; Yamamoto, Y.; Ohno, T.; Nozaki, K. *Inorg. Chem.* **2003**, *42*, 6378.
(8) (a) Griffith, J. S. *The Theory of Transition-Metal ions*; Cambridge University Press: London, 1964; p 113. (b) Khudyakov, I. V.; Serebremnikov, Y. A.; Turro, N. J. *Chem. Rev.* **1993**, *93*, 537. (c) Bendix, J.; Brorson, M.; Schaffer, C. E. *Inorg. Chem.* **1993**, *32*, 2838. (d) Sugar, J.; Musgrove, A. *J. Phys. Chem. Ref. Data* **1990**, *19*, 527. (d) Murov, S. L.; Carmichael, I.; Hug, G. L. *Handbook of Photochemistry*, 2nd ed.; Marcel Dekker: New York, 1993; p 9.
(9) Caspar, J. V. *J. Am. Chem. Soc.* **1985**, *107*, 6718.
(10) Ziolo, R. F.; Lipton, S.; Bori, Z. *J. Chem. Soc., Chem. Commun*. **1970**, 1124.
(11) Harvey, P. D.; Schaefer, W. P.; Gray, H. B. *Inorg. Chem.* **1988**, *27*, 1101.
(12) Tominaga, H.; Sakai, K.; Tsubomura, T. *J. Chem. Soc., Chem. Commun*. **1995**, 2273.
(13) Tsubomura, T.; Sakai, K. *Coord. Chem. Rev.* **1998**, *171*, 107.
(14) Kunkely, H.; Vogler, A. *Inorg. Chem. Commun.* **1999**, *2*, 533.

spectral-grade toluene were purchased from Nacalai tesque. All other reagents used were reagent grade.

(II) Instrumentation. Steady-state emission spectra were recorded using a grading monochromator (Triax 1900) with a CCD image sensor (Hamamatsu S7031). The spectral sensitivity of the spectrofluorometer was corrected using a bromine lamp (Ushio IPD 100V 500WCS). A sample in a 1 cm quartz cell was excited using an argon ion laser (488 nm, 100 mW, INNOVA 300 Coherent Co.). A cryostat (Oxford ND-1740) with a temperature controller (Oxford ITC-502) was used.

Picosecond time-resolved emission spectra were measured using a time-correlated single photon counting (TCSPC) system.[15] The second harmonic (400 nm, 10−50 mW, 80 MHz repetition rate) of a mode-locked Ti^{3+}:saphire laser (Tsunami, Spectra Physics) was used for excitation of a sample solution in a 1 mm quartz cell. The TCSPC data were recorded every 10 nm in the range 550−810 nm. One set of data was scanned for 15−30 min. Emission spectra were constructed by accumulating five sets of data. The instrumental response function (IRF) of the TCSPC system was 35 ps at the full width at half-maximum (fwhm). To determine the quantum yield of the prompt fluorescence, the second harmonic (400 nm, 700 kHz repetition rate) of a lab-made cavity-dumped mode-locked Ti^{3+}:sapphire laser was used.[15] Nanosecond pulsed lasers (Nd^{3+}: YVO_4, 532 nm, 1ns, Nanolase or Nd^{3+}: YAG, 532 nm, 5 ns, Surelight, Continuum) were used to determine the emission lifetime in the nanosecond time region. Depolarized light was used in all cases for the determination of emission quantum yields.

Subpicosecond time-resolved difference absorption spectra were obtained using laser pulses (100 fs fwhm) with a repetition rate of 200 kHz, which were generated by a mode-locked Ti^{3+}: sapphire laser with an oscillator and a regenerative amplifier (Tsunami and Spitfire, Spectra Physics, Inc.).[16] Nanosecond time-resolved difference absorption spectra were measured using the second-harmonics of the Q-switched Nd^{3+}:YAG laser (Surelight, Contiuum).[17]

(III) Determination of Emission Quantum Yield (Φ_{em}). The steady-state emission quantum yield was determined using $[Ru(bpy)_3]^{2+}$ in a deoxygenated acetonitrile solution as a reference, of which $\Phi_{em}$was determined to be 0.090 using 9,10-diphenylanthracene (DPA) (Φ_{em} = 0.91 in deaerated cyclohexane).[8d] To measure the temperature dependence of Φ_{em}, the change in concentration was corrected using the expansion coefficient of toluene.[18]

The determination of the emission quantum yield of a species with a very short lifetime was performed using TCSPC. For the platinum(0) compound, the decay of the emission at a wavenumber $\tilde{\nu}$, $I(\tilde{\nu},t)$, was well fitted to eq 1

$$I(\tilde{\nu},t) = \mathrm{IRF}(t) * \left[B_S(\tilde{\nu})\exp\left(-\frac{t}{\tau_S}\right) + B_L(\tilde{\nu})\exp\left(-\frac{t}{\tau_L}\right)\right] \quad (1)$$

where the asterisk (*) is the convolution operator and IRF(t) indicates the instrumental response function. $B_S(\tilde{\nu})$ and $B_L(\tilde{\nu})$ are intensities at $t = 0$ for the short-lived (lifetime is τ_S) and long-lived components (τ_L), respectively. The emission quantum yield of the short-lived species ($\Phi_{em,\,S}$) is given by eq 2

$$\Phi_{em,S} = \Phi_{ref}\frac{\int B'_S(\tilde{\nu})d\tilde{\nu}\cdot B_S(\tilde{\nu}_{max})\tau_S}{\int B'_{ref}(\tilde{\nu})d\tilde{\nu}\cdot B_{ref}(\tilde{\nu}_{max,ref})\tau_{ref}}\cdot\frac{1-10^{-A_{ref}}}{1-10^{-A}}\cdot\frac{n^2}{n_{ref}^2} \quad (2)$$

where Φ_{ref} is the quantum yield of the reference compound, A is the absorbance at the excitation wavelength, n is the refractive index of the solvent, and $B'_S(\tilde{\nu})$ and $B'_{ref}(\tilde{\nu})$ are normalized emission spectra of short-living species and the reference, respectively. As the emission spectra of the short-lived component were not measured in a wavenumber region lower than 1.2×10^3 cm^{-1}, the spectra were assumed to be symmetrical in calculating the area of the emission spectra. Since the emission intensity of the short-lived component was very weak, a weakly emissive 2-amminoanthraquinone was used as a secondary reference compound, of which the Φ_{em} value was determined to be 1.2×10^{-3} ($\Phi_{em} = 8 \times 10^{-3}$)[18] using a primary reference (DPA).

(IV) Computational Chemistry. Density functional calculations were carried out with the Amsterdam Density Functional program package (version 2000).[20−22] An uncontracted triple-ζ Slater-type orbital (STO) basis set with one polarization function was used for the P, C, N, and H atoms. For Pt, a triple-ζ, 5s, 5p, 5d, and 6s basis with one 6p STO was used. Zero-order regular approximation (ZORA)[23−27] was used for relativistic corrections. The core orbitals (P, 1s−2p; C, 1s; Pt, 1s−4d) were obtained as solutions of an all-electron on the isolated atom and kept frozen during the SCF calculation of the molecule. Both the local density approximation (LDA) with the parametrization of Vosko, Wilk, and Nusair (VWN)[28] and the generalized gradient approximated (GGA) potentials by Becke[29] and Perdew[30] (BP) have been employed. The calculation of excitation energy was performed using the time-dependent density functional theory (TDDFT) with BP functional.[31] TDDFT calculations using Becke's three-parameter hybrid functional (B3PW91) were also performed using GAUSSIAN 98, Rev A11.3 package.[32] Basis sets for C and H were 6-31G(d), and those for Pt and P were LANL2DZ with a relativistic effective core potential (ECP). MOLEKEL was used to draw molecular orbitals (MOs).[33] Spin−orbit integrals between singlet and triplet states have been calculated using 5d atomic-orbital coefficients obtained from the DFT calculation using ADF. All calculations were performed in the gas phase.

Results

Absorption and Emission Spectra. An intense MLCT band with an oscillator strength (f) of 0.25 appeared at 18.8

(15) Tsushima, M.; Ikeda, N.; Nozaki, K.; Ohno, T. *J. Phys. Chem. A* **2000**, *104*, 5176.
(16) Torieda, H.; Yoshimura, A.; Nozaki, K.; Sakai, S.; Ohno, T. *J. Phys. Chem. A* **2002**, *106*, 11034.
(17) Ohno, T.; Nozaki, K.; Haga, M. *Inorg. Chem.* **1992**, *31*, 548.
(18) Riddick, J. A.; Bunger, W. B.; Sakano, T. K. *Organic Solvents: Physical Properties and Methods of Purification*, 4th ed.; John Wiley & Sons: New York, 1986.
(19) Inoue, H.; Hida, M.; Nakashima, N.; Yoshihara, K. *J. Phys. Chem.* **1982**, *86*, 3184.
(20) Baerends, E. J.; Ellis, D. E.; Ros, P. *Chem. Phys.* **1993**, *2*, 42.
(21) Boerrigter, P. M.; Velde, G. te.; Baerends, E. J. *Int. J. Quantum Chem.* **1988**, *33*, 87.
(22) Velde, G. te.; Baerends, E. J. *J. Comput. Phys.* **1992**, *99*, 84.
(23) Lenthe, E. V.; Baerends, E. J.; Snijders J. G. *J. Chem. Phys.* **1993**, *99*, 4957.
(24) Lenthe, E. V.; Baerends, E. J.; Snijders J. G. *J. Chem. Phys.* **1994**, *101*, 9783.
(25) Lenthe, E. V.; Snijders J. G.; Baerends, E. J. *J. Chem. Phys.* **1996**, *105*, 6505.
(26) Lenthe, E. V.; Leeuwen, R. V.; Baerends, E. J.; Snijders J. G. *J. Quantum. Chem.* **1996**, *57*, 281.
(27) Lenthe, E. V.; Ehlers, A. E.; Baerends, E. J. *J. Chem. Phys.* **1999**, *110*, 8943.
(28) Vosko, S. H.; Wilk, L.; Nusair, M. *Can. J. Phys.* **1980**, *58*, 1200.
(29) Becke, A. D. *Phys. Rev. A* **1988**, *38*, 3098.
(30) Perdew, J. P. *Phys. Rev. B* **1986**, *33*, 8822.
(31) Gross, E. K. U.; Dobson, J. F.; Petersilka, M. In *Density Functional Theory*; Nalewajski, R. F., Ed.; Springer: Heidelberg, 1996.

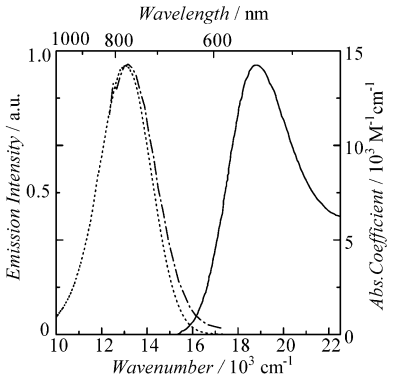

Figure 1. Absorption (—), steady-state emission (···), and short-lived component in the time-resolved emission (time window from −20 ps to 150 ps, — · · —) spectra of [Pt(binap)$_2$] in toluene at 298 K.

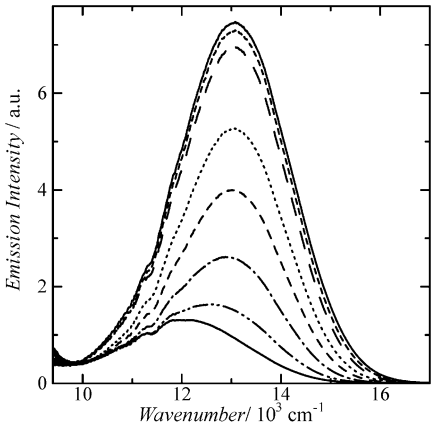

Figure 2. Emission spectra of [Pt(binap)$_2$] in toluene at various temperatures. From top to bottom: 298, 273, 253, 233, 213, 193, 173, and 153 K.

$\times$ 10^3 cm^{-1} in a toluene solution of [Pt(binap)$_2$] (the solid line in Figure 1). The steady-state emission was observed at around 13.1 $\times$ 10^3 cm^{-1} (the dotted line in Figure 1) at an ambient temperature (298 K) while a red shift of the peak and a decrease in intensity were observed by lowering the temperature from 298 to 153 K (Figure 2). The emission at 173 K peaked at 12.0 $\times$ 10^3 cm^{-1}. Figure 3 shows the time-profile of the TCSPC data at 750 nm observed when the toluene solution of the platinum(0) compound was excited with 400 nm laser light. An intense short-lived emission with a lifetime shorter than the time-resolution of the TCSPC system was followed by a long emission component. The emission spectrum for the short-lived component was

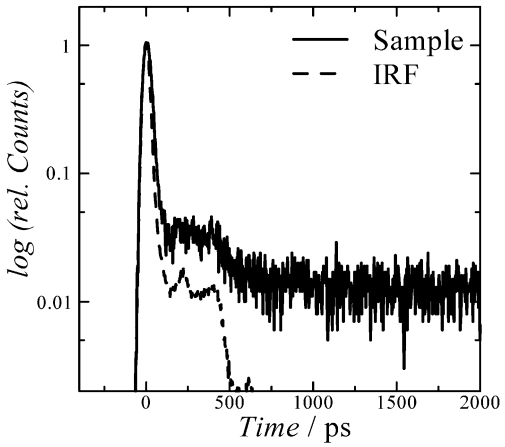

Figure 3. Time-profile of TCSPC data at 750 nm for [Pt(binap)$_2$] in deaerated toluene solution with excitation at 400 nm (—). The instrumental response function of the TCSPC system was shown by dashed line (- - -).

obtained by integrating the photons in the time range from −20 to 150 ps at each wavelength (the dashed−dotted line in Figure 1). The resulting emission spectrum was very similar to the steady-state emission spectrum (the dotted line in Figure 1). The quantum yield of the short-lived component ($\Phi_{em,S}$) was 1.56 $\times$ 10^{-4}, about 10^3 times smaller than the total emission quantum yield (Φ_{em} = 0.12 at 298 K in toluene). The value of Φ_{em} in CH_2Cl_2 was $^1/_{10}$ of that in toluene although $\Phi_{em,S}$ was almost identical to that in toluene (Table 1). The photophysical properties of the platinum(0) compound are summarized in Table 1. Figure 4 shows the time-profile of emission at 750 nm. The lifetime of the longer component (τ_L) was similar to that reported previously (1.48 μs) in a benzene solution at 293 K.[12] The values of τ_L varied remarkably with the solvent: 1.25 μs in toluene, 0.38 μs in tetrahydrofuran, 0.18 μs in CH_2Cl_2, 0.095 μs in acetonitrile. The luminescence of [Pt(binap)$_2$] was quenched by oxygen in benzene, and the generation of singlet oxygen was confirmed by observing its luminescence at around 1270 nm. Therefore, the excited state exhibiting the long-lived luminescence was assigned as triplet state.[34]

We measured the values of τ_L and Φ_{em} at various temperatures ranging from 153 to 298 K in toluene. With decreasing temperature, the τ_L value increased whereas the Φ_{em}value decreased as shown in Table 2. The radiative rates for the long-lived component ($k_{r,L}$) were obtained from Φ_{em} and τ_L because Φ_{em} is mainly dominated by the long-lived component. The $k_{r,L}$ values of 9.9 $\times$ 10^4 s^{-1} at 298 K decreased to 3.0 $\times$ 10^3 s^{-1} at 153 K (Table 2), suggesting that the fast radiative process at higher temperatures will be replaced by a slow process at lower temperatures.

Transient Absorption Spectra. Figure 5a shows the subpicosecond time-resolved transient absorption spectra observed for [Pt(binap)$_2$] in toluene with excitation at 400 nm. Bleaching observed at around 530 nm is due to the disappearance of the MLCT band in the excited state. In a time region from 0 to 3 ps, bleaching was also observed at around 750 nm where the ground-state absorption was absent.

(32) Frisch, M. J.; Trucks, G. W.; Schlegel, H. B.; Scuseria, G. E.; Robb, M. A.; Cheeseman, J. R.; Zakrzewski, V. G.; Montgomery, J. A., Jr.; Stratmann, R. E.; Burant, J. C.; Dapprich, S.; Millam, J. M.; Daniels, A. D.; Kudin, K. N.; Strain, M. C.; Farkas, O.; Tomasi, J.; Barone, V.; Cossi, M.; Cammi, R.; Mennucci, B.; Pomelli, C.; Adamo, C.; Clifford, S.; Ochterski, J.; Petersson, G. A.; Ayala, P. Y.; Cui, Q.; Morokuma, K.; Malick, D. K.; Rabuck, A. D.; Raghavachari, K.; Foresman, J. B.; Cioslowski, J.; Ortiz, J. V.; Stefanov, B. B.; Liu, G.; Liashenko, A.; Piskorz, P.; Komaromi, I.; Gomperts, R.; Martin, R. L.; Fox, D. J.; Keith, T.; Al-Laham, M. A.; Peng, C. Y.; Nanayakkara, A.; Gonzalez, C.; Challacombe, M.; Gill, P. M. W.; Johnson, B. G.; Chen, W.; Wong, M. W.; Andres, J. L.; Head-Gordon, M.; Replogle, E. S.; Pople, J. A. *Gaussian 98*, revision A.11.3; Gaussian, Inc.: Pittsburgh, PA, 1998.

(33) (a) Flukiger, P.; Luthi, H. P.; Portmann, S.; Weber, J. *Swiss Center for Scientific Computing*; Manno, Switzerland, 2000−2002. (b) Portmann, S.; Luthi, H. P. MOLEKEL: An Interactive Molecular Graphics Tool. *Chimia* **2000**, *54*, 766.

(34) Tsubomura, T.; Abe, M.; Tarutani, M.; Yamada, H.; Tsukuda T. *Bull. Chem. Soc. Jpn.* **2003**, *76*, 2151.

Table 1. Photophysical Data of Long-Lived and Short-Lived Emission Components at 298 K

			long-lived		short-lived		
solvent	$\tilde{\nu}_{em}^{max}/10^3$ cm^{-1}	Φ_{em}	τ_L/μs	$\Phi_{em}\tau_L^{-1}$/s^{-1}	$\Phi_{em,S}$[a]	τ_S/ps	$\Phi_{em,S}\tau_S^{-1}$/s^{-1}
toluene	13.1	0.12[c]	1.25	9.9×10^4	1.56×10^{-4}	3.2[b]	4.9×10^{7}[b]
CH_2Cl_2	12.9	0.0099	0.18	5.5×10^4	1.62×10^{-4}	<17	$>1 \times 10^7$
acetonitrile	12.8	0.0090	0.095	9.5×10^4			

[a] Determined with excitation at 400 nm. [b] Determined from the decay (at 750 nm) analysis of subpicosecond transient absorption spectra. [c] The previously reported Φ_{em}value of 0.024 in a benzene solution[12] should be much smaller than the actual value. This is probably due to incomplete deoxygenation. In the previous study, the Φ_{em} value and the lifetime were determined in separate runs. The reported lifetime of 1.48 μs was reproduced in this work.

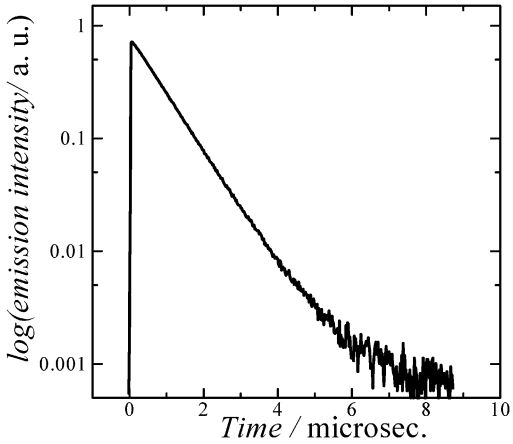

Figure 4. Time-profile of emission at 750 nm in a microsecond time region in deaerated toluene solution with excitation at 532 nm.

Table 2. Total Quantum Yields (Φ_{em}'s) and the Lifetimes (τ_L's) of a Long-Lived Emission Component in Toluene at Various Temperatures

T/K	Φ_{em}	τ_L/μs	$k_{r,L}/10^4$ s^{-1}
298	0.124	1.25	9.92
273	0.102	1.9	5.5
253	0.087	2.7	3.3
233	0.073	3.7	2.0
213	0.058	4.8	1.2
193	0.045	6.3	0.72
173	0.032	7.8	0.41
153	0.022	7.9	0.30

The similarity in shape between the negative absorption band (shaded area in Figure 5a) and the emission spectrum of the short-lived component (dash−dotted line in Figure 1) indicates that the apparent bleaching at 750 nm can be attributed to the stimulated emission corresponding to the short-lived emission detected by the TCSPC. The lifetime of the stimulated emission at 750 nm was determined to be 3.2 ps (Figure 5b). The stimulated emission of ^{1}MLCT has been observed only for [Ru(bpy)$_2$(dcbpy)] adsorbed on SnO_2 nanocrystal by now.[2]

The transient absorption spectra of the Pt(0) compound showed absorption bands at around 450, 620, and 900 nm. These features in the absorption spectrum are similar to those observed for the chemically prepared 1,1′-binaphthyl anion radical: absorption bands appeared at 450 and 650 nm, and in the near-infrared region (900−2000 nm).[35] The presence of the anion radical of 1,1′-binaphthyl moiety supports the assignment that the excited state is a Pt(0)-to-binap charge transfer state (MLCT).

(35) Shida, T. Electronic absorption spectra of radical ions; Elsevier Science Publishers: B.V., 1988.

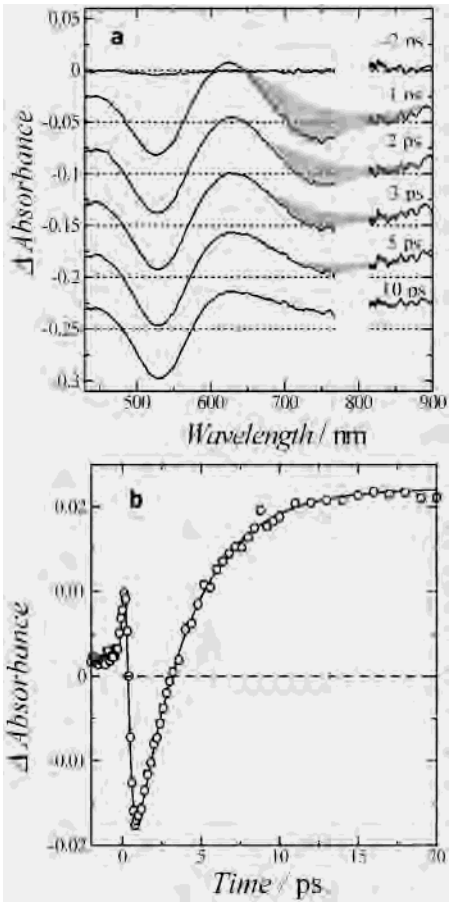

Figure 5. Subpicosecond time-resolved transient absorption spectra of [Pt(binap)$_2$] in toluene (a) and the time-profile of the transient absorption at 750 nm (b). The solid line in (b) is the curve fitted using three exponential functions with convolution of the instrumental function (fwhm = 0.4 ps): very fast decay with the time constant less than 0.4 ps, a rise with 3.2 ps, and a decay with 1.2 μs. The first component might be due to excitation of the solvent.

The lifetime of the transient absorption was 1.1 μs in toluene at 298 K, in agreement with the lifetime of the luminescence.

Quantum Chemical Calculations. To understand the photophysical properties of the MLCT states of the platinum-(0) compound, theoretical analyses based on the information obtained using DFT were performed. To ascertain the quality of the DFT calculation, the geometry calculated by DFT was compared with that obtained from the X-ray analysis.[12] Since the X-ray structure showed quasi-D_2 symmetry, all the DFT calculations in this work were performed under D_2 symmetry. Most of the bond lengths and the angles were in good agreement with those observed with less than 2% error. The observed bond length of Pt−P was 233 pm whereas the

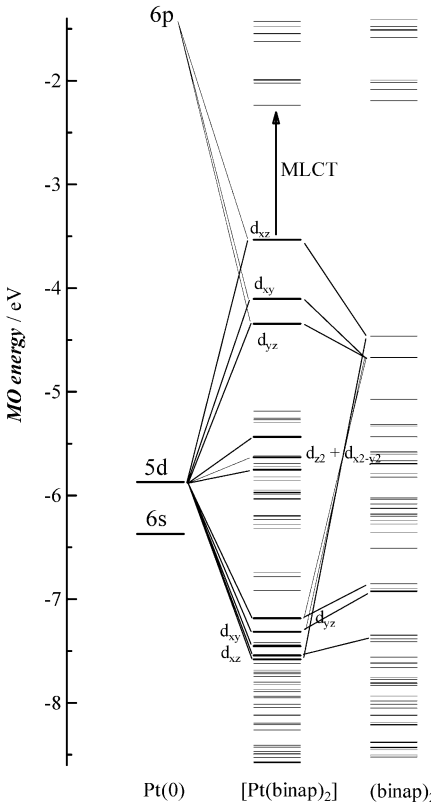

Figure 6. The orbital correlation between the fragments of Pt(0) and bis-(binap) into [Pt(binap)$_2$] at the MLCT geometry. MO levels with thick lines contain >10% d-orbital contributions.

calculated length was 237 pm. The average bite angle of P_1-Pt-P_2 was 92.0°, and the calculated angle was 93.3°. The observed dihedral angle between two planes of P_1-Pt-P_2 and P_3-Pt-P_4 (dha) was 90°, and the calculated dha was 89.6°.

The geometries of the lowest ^{3}MLCT and $[Pt(I)(binap)_2]^+$ were also obtained using DFT. A close resemblance in structure was found between the ^{3}MLCT and the Pt(I) compound with d^9 configuration as seen for the copper(I) diimine compound in the previous study,[7] indicating that the geometry at the ^{3}MLCT is dominated by the nature of the d^9 configuration. The calculated bond lengths of Pt−P were 243 pm (^{3}MLCT) and 242 pm (Pt(I)), slightly longer than that of the Pt(0) (237 pm) in the ground state (GS). The P_1-Pt-P_2 bite angles were 89.4° (^{3}MLCT) and 90.0° (Pt(I)), smaller than that of Pt(0) (93.3°). The dha was 84.1° (^{3}MLCT) and 83.8° (Pt(I)), and the change in dha between the MLCT and the GS was 5.5°. In this work, we investigated the photophysical properties of ^{1}MLCT using ^{3}MLCT geometry since accurate geometry at the ^{1}MLCT could not be obtained using the current DFT package. The difference in geometry between ^{1}MLCT and ^{3}MLCT is negligible because the coordination structure is dominated by the d^9 configuration and the excited electron is spread over two binap ligands in both cases.

Figure 6 shows the orbital correlation between [Pt(binap)$_2$] and the fragments of Pt(0) and (binap)$_2$ in MLCT geometry. The HOMO, HOMO − 1, and HOMO − 2 are antibonding orbitals between occupied orbitals and 5d$_{xz}$, 5d$_{xy}$, and 5d$_{yz}$,

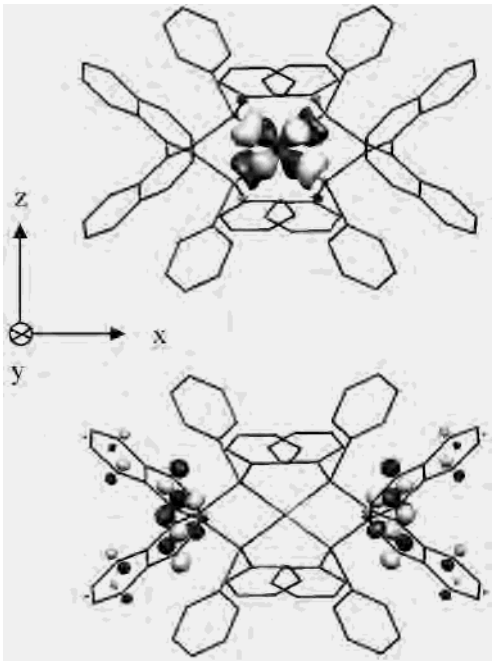

Figure 7. HOMO (58b$_2$; upper) and LUMO (59b$_1$; lower) of [Pt(binap)$_2$].

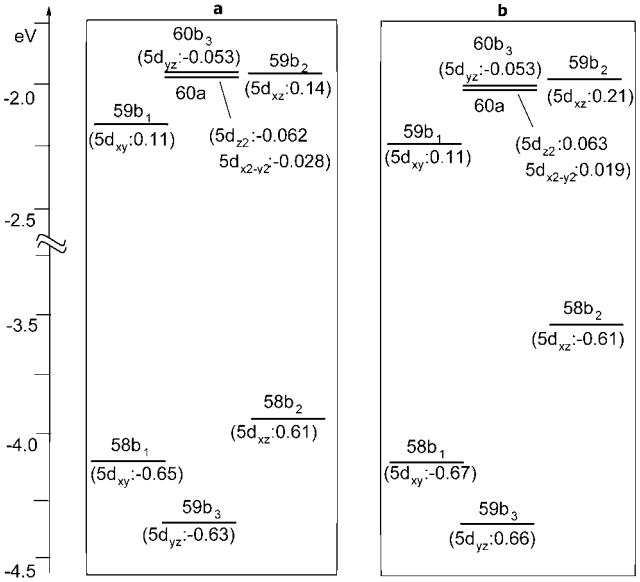

Figure 8. MO energy level at the ground state (a) and at the MLCT geometry (b). Coefficients of d-orbitals in each MOs are given in parentheses.

respectively. The corresponding bonding orbitals are located at around −7.5 eV. Figure 7 shows the HOMO and LUMO. The HOMO (58b$_2$, 58th MO with b$_2$ symmetry) mainly consists of 5d (31%) and 6p (8%) of Pt, 3s, 3p, and 3d (32%) of P, and 2p (13%) of C in the phenyl groups. On the other hand, LUMO (59b$_1$, 59th MO with b$_1$ symmetry) has about 80% contributions of 2p of C of naphthyl groups, 2% of 3d of P, and only 1% of 5d of Pt.

Figure 8a and b show the MO energy levels obtained as the singlet ground state in the GS and MLCT geometries, respectively. At the GS geometry, the energy difference between HOMO (58b$_2$) and HOMO − 1 (58b$_1$) is only 1×10^3 cm^{-1} whereas it is considerably increased to about 4.6×10^3 cm^{-1} in the MLCT geometry despite small geometry

Table 3. Excitation Energy (E_{ex}), Oscillator Strength (f), and Spin−Orbit Integral (SOI)[a] with the Lowest ^{3}MLCT (1^3B_3: $58b_2 \rightarrow 59b_1$) at the MLCT Geometry[36]

^{1}MLCT transition (contribution)	$E_{ex}/10^3$ cm^{-1} (f)	SOI[a]/cm^{-1}
1^1B_3: $58b_2 \rightarrow 59b_1$ (0.98)	11.8 (0.16), 15.4 (0.12)[b]	0
	14.5 (0.21),[c] 19.7 (0.17)[d]	
1^1B_2: $58b_2 \rightarrow 60a$ (0.99)	12.6 (8.4×10^{-3})	8
1^1B_1: $58b_2 \rightarrow 60b_3$ (1.00)	12.8 (5.2×10^{-3})	12
2^1A: $58b_2 \rightarrow 59b_2$ (0.96)	13.7 (0)	46
3^1A: $58b_1 \rightarrow 59b_1$ (1.00)	15.3 (0)	843
2^1B_1: $59b_3 \rightarrow 59b_2$ (1.00)	15.5 (4.7×10^{-3})	0
2^1B_3: $58b_2 \rightarrow 60b_1$ (0.99)	16.2 (3.4×10^{-2})	0
2^1B_2: $58b_2 \rightarrow 61a$ (0.99)	16.7 (1.4×10^{-3})	33
3^1B_1: $58b_1 \rightarrow 60a$ (1.00)	16.9 (1.6×10^{-3})	0
3^1B_2: $58b_1 \rightarrow 60b_3$ (0.94)	17.1 (1.7×10^{-8})	0
4^1B_2: $59b_3 \rightarrow 59b_1$ (0.56)	17.2 (1.9×10^{-3})	835
$58b_2 \rightarrow 62a$ (0.36)		20
3^1B_3: $58b_1 \rightarrow 59b_2$ (1.00)	17.4 (2.3×10^{-6})	0
5^1B_2: $58b_2 \rightarrow 62a$ (0.60)	17.4 (8.4×10^{-3})	20
$59b_3 \rightarrow 59b_1$ (0.39)		835

[a] $|\langle\Phi_{^1MLCT}|H_{SO}|\Phi_{1^3B_3}\rangle|$. [b] Using BP at the GS geometry. [c] Using B3PW91 at the MLCT geometry. [d] Using B3PW91 at the GS geometry.

changes. The reason for the large splitting in the MLCT geometry is that the energy level of HOMO increases due to increased antibonding interactions between d_{xz} and an occupied MO of binap whereas the energy level of HOMO − 1 remains almost unchanged. The increase in HOMO energy is caused by an increment of 15% in the overlap integral between $5d_{xz}$ and the binap orbitals on changing from the GS to the MLCT geometry (from −0.179 to −0.205). On the other hand, the overlap between d_{xy} and the binap orbitals is smaller than that between d_{xz} and the binap orbitals: the change in the overlap integral is only 4% (from −0.158 to −0.151). One reason for the weaker interactions between the d_{xy} and the binap orbital seems to be the smaller overlap between d_{xy} and 3p on P.

Table 3 shows the excitation energies and oscillator strengths (f) of ^{1}MLCT transitions. The lowest MLCT involves an electronic transition, $58b_2 \rightarrow 59b_1$ (1^1B_3), and has the highest oscillator strength among lower-lying MLCT transitions. In the GS geometry, the excitation energies to 1^1B are calculated to be 15.7×10^3 cm^{-1} with an oscillator strength of 0.12 using the BP functional of ADF and 19.7×10^3 cm^{-1} with 0.17 using a hybrid DFT (B3PW91) of g98. Thus, the excitation energy and the f value calculated using a hybrid DFT were in better agreement with the observed levels (18.8×10^3 cm^{-1} and 0.25). The excitation energy of this transition decreased to 11.8×10^3 cm^{-1} (BP) or 14.5×10^3 cm^{-1} (B3PW91) in the MLCT geometry while the oscillator strengths increased to 0.16(BP) or 0.21-(B3PW91). The direction of the transition dipole is along the x−axis depicted in Figure 7, the longest C_2 axis of the molecule. The energy gaps between 1^1B_3 and the lowest ^{3}-MLCT(1^3B_3) are calculated to be 1.48×10^3 cm^{-1} (BP).

Discussion

Assignment of Emitting States. It is of significant interest to assign the short-lived emissive state that seems responsible for the strong steady-state emission at ambient temperature. The reported radiative rate constants (k_r) of ^{3}MLCT are up to less than 10^6 s^{-1}: 4.6×10^5 s^{-1} for $[Ru(bpy)_3]^{2+}$,[37] 2.5×10^5 s^{-1} for $[Re(bpy)(CO)(py)]^+$ (py = pyridine),[38] 1×10^5 s^{-1} for $[Os(bpy)_3]^{2+}$,[39] 2×10^5 s^{-1} for $[Ir(ppy)_3]$ (ppy = 2-phenylpyridine).[40] These values were obtained from the lifetimes and steady-state emission quantum yields in the literature. The observed value of $k_{r,S}$ for this short-lived emission of the Pt(0) compound is as large as 4.9×10^7 s^{-1} in toluene (Table 1). Furthermore, the observed $k_{r,S}$ is in good agreement with that (3×10^7 s^{-1}) calculated from the oscillator strength of the MLCT absorption band (0.25). Therefore, the short-lived emission is assigned to the prompt fluorescence corresponding to the intense MLCT band at around 18.8×10^3 cm^{-1}.

Scheme 1. Two Emitting States[a]

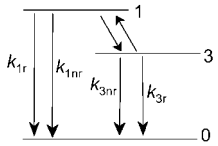

[a] 1 indicates ^{1}MLCT, 3 indicates ^{3}MLCT, and 0 indicates ground state. Solid arrows are radiative paths and dashed-arrows are nonradiative paths.

The temperature dependence of the emission spectra of the Pt(0) compound resembles that of copper(I) bis(diimine) compounds.[7] We analyzed the temperature dependence of $\Phi_{em}\tau_L^{-1}$ using the two-state model depicted in Scheme 1 which was proposed by McMillin to explain the temperature-dependent emission spectra of copper(I) compounds.[41] When states 1 and 3 are in equilibrium,[42] the ratio of the populations of state 1 and state 3 is approximated using a pseudoequilibrium constant (K) which is simply expressed using their degeneracy (g_1 and g_3) and the energy difference (ΔE).[41]

$$K = \frac{g_1}{g_3}\exp\left(-\frac{\Delta E}{RT}\right) \tag{3}$$

By neglecting the prompt fluorescence, the magnitude of $\Phi_{em}\tau_L^{-1}$ is given by eq 4 as a function of the pseudoequilibrium constant (K)

$$\frac{\Phi_{em}}{\tau_L} = \frac{k_{1r}K + k_{3r}}{1 + K} \tag{4}$$

(36) For the nomenclature of electronic states, we used the form of (the order from the lowest energy in the states with the same symmetry and spin)(spin state)(symmetry of the wave function in D_2 point group) for electronic states free from effects of spin−orbit coupling. For examples, 3^1B_3 means the third electronic state with singlet state and with B_3 symmetry. The state produced from the lowest ^{3}MLCT by considering spin−orbit coupling was identified using its symmetry of wave function including spin space.

(37) Harrigan, R. W.; Hager, G. D.; Crosby, G. A. *Chem. Phys. Lett.* **1973**, *21*, 487.
(38) Sacksteder, L. A.; Zipp, A. P.; Brown, E. A.; Streich, J.; Demas, J. N.; DeGraff, B. A., *Inorg. Chem.* **1990**, *29*, 4335.
(39) Lumpkin, R. S.; Meyer, T. J. *J. Phys. Chem.* **1986**, *90*, 5307.
(40) Colombo, M. G.; Brunold, T. C.; Riedener, T.; Gudel, H. U.; Fortsch, M.; Burgi, H. B. *Inorg. Chem.* **1994**, *33*, 545.
(41) Kirchhoff, J. R.; Gamache, R. E.; Blaskie, M. W.; Paggio, A. D.; Lengel, R. K.; McMillin, D. R. *Inorg. Chem.* **1983**, *22*, 2380.
(42) The condition for the equilibrium between states 1 and 3 is ($k_{1r} + k_{1nr}$) < k_{13}. This condition was easily confirmed by the facts that no fast recovery of the bleaching of the MLCT band was observed during the decay of the ^{1}MLCT in the transient absorption spectra shown in Figure 5a; namely, the ^{1}MLCT was efficiently converted to the ^{3}-MLCT.

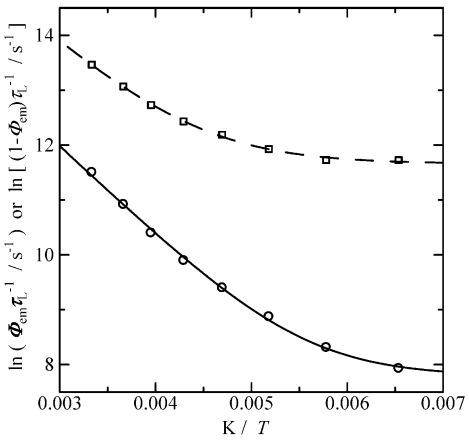

Figure 9. Plot of $\ln(\Phi_{em}\tau_L^{-1})$ versus T^{-1} (○) and $\ln[(1-\Phi_{em})\tau_L^{-1}]$ versus T^{-1} (□). The solid and the broken lines were obtained from eqs 4 and 11, respectively, using the parameters obtained by nonlinear least-squares method.

where k_{1r} and k_{3r} are radiative rate constants of ^{1}MLCT and ^{3}MLCT, respectively.

The logarithm plot of $\Phi_{em}\tau_L^{-1}$ against the inverse of temperatures was analyzed by a nonlinear least-squares curve fitting method assuming that k_{1r} and k_{3r} are temperature independent, $g_1 = 1$ and $g_3 = 3$ (Figure 9). The analysis provided $k_{1r} = 6.7 \times 10^7$ s^{-1}, $k_{3r} = 2.4 \times 10^3$ s^{-1}, and $\Delta E = 1.15 \times 10^3$ cm^{-1}. The value of k_{3r} may contain some errors due to the lack of data at temperature regions lower than 150 K. The radiative rate constant k_{1r} of the upper-lying state is in good agreement with the value of $k_{r,S}$ (4.9×10^7 s^{-1}) directly obtained from the short-lived emission. The ΔE is also in excellent agreement with the difference in peak energy between the prompt fluorescence and the phosphorescence at 153 K (1.1×10^3 cm^{-1}).

The following two findings indicate that the long-lived emission at ambient temperature is mainly dominated by delayed fluorescence. (1) The emission intensity decreased and the peak red-shifted by lowering the temperature (Figure 2), and (2) the steady-state emission spectrum at ambient temperature was almost identical to that of the prompt fluorescence. Consequently, both the prompt and the delayed fluorescence involve the same radiative process, that is, $1^1B_3 \rightarrow$ GS. The observed energy gap between ^{3}MLCT and ^{1}MLCT (1.2×10^3 cm^{-1}) is smaller than the calculated gap of 1.48×10^3 cm^{-1}. The emission appearing at around 12×10^3 cm^{-1} at 153 K had a radiative rate of 2.7×10^3 s^{-1} and is assigned to phosphorescence from ^{3}MLCT.

Stokes Shift of the Fluorescence. The MLCT transition of d^{10} metal compounds involves a change in electron configuration to d^9, which is accompanied by structural changes due to the Jahn−Teller effect.[43] This explains why the MLCT fluorescence in d^{10} metal compounds shows a fairly large Stokes shift: 5.7×10^3 cm^{-1} for $[Pt(binap)_2]$ and 5.4×10^3 cm^{-1} for $[Cu(dmp)_2]^+$. The DFT calculation of the platinum(0) compound indicated that the changes in the coordination structure at the MLCT were not so large as those for $[Cu(dmp)_2]^+$: the dha between two P−Pt−P planes was reduced by about 6° while the dha between two N−Cu−N planes decreased by ca. 20°.[7] The Stokes shift was calculated as the difference between the excitation energy to 1^1B_3 in the GS geometry and in the MLCT geometry, which was 3.6×10^3 cm^{-1} using BP, a little smaller than that observed. A more sophisticated hybrid DFT (B3PW91) gave 5.2×10^3 cm^{-1}, which is in agreement with that observed (5.7×10^3 cm^{-1}).

Intersystem Crossing (ISC) Rate. The ^{1}MLCT lifetimes of transition metal compounds are presumed to be dominated by the rates of intersystem crossing (ISC) which are enhanced by the large spin−orbit coupling of d electrons, at least more than several hundred wavenumbers.[8] The lifetime of a fluorescent MLCT state in $[Ru(II)(bpy)_3]^{2+}$ was observed to be 40 ± 15 fs.[3] We pointed out in the previous study,[7] however, that the lifetime of ^{1}MLCT in copper(I) bis(diimine) compounds was 15 ps, much longer than that of $[Ru(bpy)_3]^{2+}$, although the spin−orbit coupling constant of 3d electron in Cu(I) (829 cm^{-1}) is almost identical to that of 4d electron in Ru(II) (990 cm^{-1}).[8] This study also demonstrated that the lifetime of ^{1}MLCT in $[Pt(binap)_2]$ (3.2 ps) was not so short as expected from the large spin−orbit coupling constant of 5d electron of Pt (4000 cm^{-1}).[8] Thus, it is necessary to evaluate the strength of the spin−orbit interaction that actually induces the ISC in the Pt(0) compound.

Here we considered ISC induced by direct spin−orbit interaction between the lowest ^{1}MLCT(1^1B_3) and ^{3}MLCT states. Under Born−Oppenheimer approximation, the ISC rate is expressed simply as the product of the square of the spin−orbit integral, $\langle {}^3\Phi_n|H_{SO}|{}^1\Phi_m\rangle$, and FCWD (Franck−Condon-weighted density of final vibronic states)[7,44,45]

$$k(^1\mathrm{MLCT}_m \rightarrow {}^3\mathrm{MLCT}_n) = \frac{2\pi}{\hbar}|\langle {}^3\Phi_n|H_{SO}|{}^1\Phi_m\rangle|^2\mathrm{FCWD} \quad (5)$$

where $\mathrm{FCWD} = |\langle\chi_n|\chi_m\rangle|^2\rho(E_{^3\mathrm{MLCT}} = E_{^1\mathrm{MLCT}})$.

Here, Φ and χ are an electronic wave function and a vibrational wave function, respectively, and $\rho(E_{^3\mathrm{MLCT}} = E_{^1\mathrm{MLCT}})$ is the density of the final vibronic states having the same energy as the initial states. The details of the calculation of spin−orbit integrals between MLCT states, $\langle\Phi_a|H_{so}|\Phi_b\rangle$, are described elsewhere.[7] Briefly, the integrals were obtained using one-electron spin−orbit operator $H_{SO} = \zeta \sum_i^{Nel} l_i \cdot s_i$ with spin−orbit coupling with light atoms (H, C, N, P) being ignored. Under these assumptions, the spin−orbit integrals between two excited states are reduced to those between two 5d atomic orbitals centered on platinum(0) and thus calculated using the coefficients of 5d involved in the MOs shown in Figure 8b and using $\varsigma_{5d}(Pt) = 4000$ cm^{-1}.[46]

(43) Cotton, F. A.; Wilkinson, G. *Advanced Inorganic Chemistry*; John Wiley & Sons: New York, 1962.

(44) (a) Siebrand, W. *Chem. Phys. Lett.* **1970**, *6*, 192. (b) Lawetz, V.; Orlandi, G.; Siebrand, W. *J. Chem. Phys.* **1972**, *56*, 4058.

(45) See textbook on quantum mechanics, e.g.: Landau, L. D.; Lifschitz, E. M.; *Quantum Mechanics (Non-Relativistic Theory)*, 3rd ed.; Pergamon Press: Oxford, England, 1977.

(46) In these calculations, the spin−orbit coupling due to the 3p electrons in phosphorus ($\varsigma_{3p} = 299$ cm^{-1})[8] has been neglected because it was much smaller compared to the contribution from 5d electrons: the largest spin−orbit integral due to the 3p electrons is 8 cm^{-1} for the ISC channel $1^1B_3 \rightarrow 2^3A$ whereas these values are less than 0.3 cm^{-1} for all the other ISC channels.

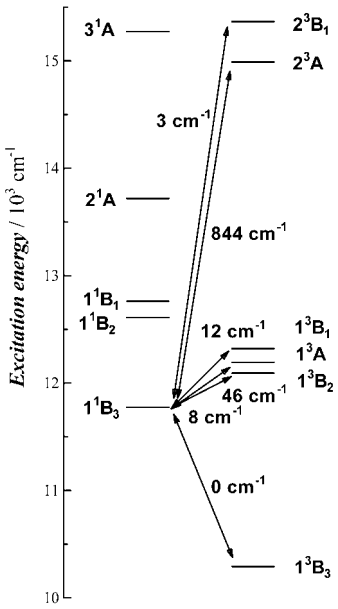

Figure 10. Spin−orbit integral from the lowest singlet (1^1B_3) to triplet states at the MLCT geometry of [Pt(binap)$_2$].

The spin−orbit integrals between the lowest ^{1}MLCT (1^1B_3: $58b_2 \rightarrow 59b_1$) and ^{3}MLCT are shown in Figure 10. Although 1^1B_3 interacts strongly with 2^3A ($58b_1 \rightarrow 59b_1$), the spin−orbit integral of which is 844 cm^{-1}, 2^3A lies 3.2 $\times$ 10^3 cm^{-1} higher than 1^1B_3. Therefore, the ISC channel $1^1B_3 \rightarrow 2^3A$ is strongly endothermic and thus possesses very small FCWD in eq 5. The ISC channel from 1^1B_3 to the lowest ^{3}MLCT state (1^3B_3: $58b2 \rightarrow 59b_1$) is energetically favorable but symmetrically forbidden. Possible ISC channels due to direct spin−orbit interaction are therefore from 1^1B_3 to the lower-lying triplet states (1^3B_2, 1^3A, and 1^3B_1). All of these ISC channels are induced by the spin−orbit integrals between π^* orbitals, which are less than 50 cm^{-1}.

In [Ru(bpy)$_3$]$^{2+}$, HOMO(dπ_{a1}) lies 2.4 $\times$ 10^3 cm^{-1} above degenerate HOMO − 1 (dπ_{e-1} and dπ_{e-2}).[47] Since these t_{2g} orbitals are nonbonding, the structural change on MLCT formation is quite small. The spin−orbit integral between dπ_{a1} and dπ_e is calculated to be ca. 300 cm^{-1} from Table 3 in ref 47 and ζ = 990 cm^{-1} and that between dπ_{e-1} and dπ_{e-2} is ca. 200 cm^{-1}. The former spin−orbit integral works in the slightly uphill (ca. 1000 cm^{-1}) ISC $^1A_2$(d$\pi_{a1}\rightarrow\pi^*a_2$) $\rightarrow$ ^3E(d$\pi_e\rightarrow\pi^*a_2$) and the latter induces the downhill ISC ^1E(d$\pi_e\rightarrow\pi^*a_2$) $\rightarrow$ ^3E(d$\pi_e\rightarrow\pi^*a_2$), shortening the lifetime of ^{1}MLCT to the femtosecond time region. On the other hand, the structural changes in the MLCT of [Pt(binap)$_2$] cause large energy splitting of about 4.6 $\times$ 10^3 cm^{-1} between HOMO and HOMO − 1, thereby making ISC channels involving both HOMO and HOMO − 1 energetically unfavorable. Consequently, the relatively slow ISC channels induced by spin−orbit integrals due to the small contribution of d-orbitals in LUMO and LUMO + 1 are dominant in the Pt(0) compound.

The spin−orbit integral between HOMO and HOMO − 1 in [Ru(bpy)$_3$]$^{2+}$ is ca. 300 cm^{-1}, 6 times as strong as that in [Pt(binap)$_2$] (46 cm^{-1}). In [Cu(I)(dmp)$_2$]$^+$ compounds, the spin−orbit integrals of the possible ISC channels were 26 cm^{-1}. As seen from eq 5, the ISC rate is proportional to the square of the spin−orbit integral if the difference in FCWD is ignored. It is worth noting that the relative magnitude of k_{ISC} observed in [Ru(bpy)$_3$]$^{2+}$, [Pt(binap)$_2$], and [Cu(dmp)$_2$]$^+$ (80:1:0.2) demonstrates a good relationship to that of the square of the spin−orbit integral of the possible ISC channels (43:1:0.32), not to that of spin−orbit coupling constants of the central metal ions (ζ_{Ru}:ζ_{Pt}:ζ_{Cu} = 1:4:0.8).[8]

Scheme 2. Splitting of the Lowest ^{3}MLCT (1^3B_3) by Second-Order Spin−Orbit Interaction

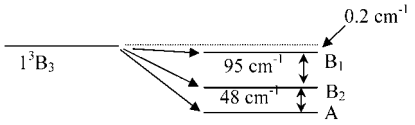

Properties of the Phosphorescent State. The emission that appeared at around 12.0 $\times$ 10^3 cm^{-1} at 153 K (Figure 2) has been assigned as the phosphorescence. The radiative rate constant was 2.4 $\times$ 10^3 s^{-1} as described above. The excitation energy to the lowest ^{3}MLCT was calculated as 10.3 $\times$ 10^3 cm^{-1} using the BP functional without spin−orbit interaction. The triplet state is perturbed by various singlet states when spin−orbit interaction occurs. The lowest triplet state (1^3B_3) is split into three states, A, B_1, and B_2, by second-order spin−orbit interaction with ^{1}A, $^1B_1$, and $^1B_2$, respectively. The energy of each state can be calculated using zeroth-order eigenfunction Φ and zeroth-order eigenvalue E of Hamiltonian without spin−orbit interaction[48]

$$E_{A,B_1,B_2} = E_{1^3B_3} + \sum_n \frac{H_{13}H_{31}}{E_{1^3B_3} - E_{n^1A,n^1B_1,n^1B_2}} |\langle \chi_{n^1A,n^1B_1,n^1B_2} | \chi_{1^3A} \rangle|^2 \quad (6)$$

where $H_{13} = \langle \Phi_{n^1A,n^1B_1,n^1B_2} | H_{SO} | \Phi_{1^3B_3} \rangle$ and $H_{31} = \langle \Phi_{1^3B_3} | H_{SO} | \Phi_{n^1A,n^1B_1,n^1B_2} \rangle$. The overlap integrals between the vibrational wave functions (χ) were assumed to be unity in the following calculations. The resulting splitting due to second-order spin−orbit perturbation is shown in Scheme 2. The lowest MLCT is A which resides 48 cm^{-1} lower than that of B_2 and is situated 143 cm^{-1} lower than 1^3B_3. The radiative rate constants of phosphorescence can be calculated using the following expression[48]

$$k_r = \frac{16\pi^3 \times 10^6 \times \tilde{\nu}^3}{3h\epsilon_0} |M_{T\rightarrow GS}|^2 \quad (7)$$

where $\tilde{\nu}$ is the excitation energy of the triplet state, h and ϵ_0 are Planck's constant and vacuum permittivity, respectively. The transition moment $M_{T\rightarrow GS}$ for phosphorescence is calculated using the first-order perturbation theory[48]

(47) Daul, C.; Baerends, E. J.; Vernooijs, P. *Inorg. Chem.* **1994**, *33*, 3538.

(48) McGlynn, S. P.; Azumi, T.; Kinoshita, M.; *Molecular Spectroscopy of The Triplet State*; Prentice-Hall: Englewood Cliffs, NJ, 1969.

$$M_{T\rightarrow GS} = \sum_n M_{n^1A,n^1B_1,n^1B_2\rightarrow GS} \times \frac{|H_{13}|}{E_{1^3A} - E_{n^1A,n^1B_1,n^1B_2}} |\langle \chi_{n^1A,n^1B_1,n^1B_2} | \chi_{1^3A} \rangle| \quad (8)$$

The transition moments for ^{1}MLCT in eq 8 were calculated from the oscillator strength (f) and the excitation energy in Table 3.[49] The radiative rate constants, k_r, calculated for $B_1 \rightarrow$ GS and $B_2 \rightarrow$ GS are 6.1 s^{-1} and 1.2 $\times$ 10^3 s^{-1}, respectively, whereas the radiative transition A $\rightarrow$ GS is symmetrically forbidden. Since the energy difference between A and B_2 is only 48 cm^{-1} (69 K), the emission from B_2 seems to play a dominant role in phosphorescence above 150 K. Thus, these results are consistent with the k_r value of 2.7 $\times$ 10^3 s^{-1} determined from the temperature-dependent emission properties in a range from 300 to 150 K. An accurate assessment of our theoretical calculation requires analysis of the emission intensity at temperatures lower than 50 K.

The transition dipole moment for $B_2 \rightarrow$ GS transition comes largely from that of $4^1B_2 \rightarrow$ GS transition. Although the spin−orbit integral between 1^3B_3 and 4^1B_2 is significant (835 cm^{-1}), the large energy difference between these states (6.9 $\times$ 10^3 cm^{-1}) reduces the extent of mixing due to spin−orbit interaction, thereby decreasing the radiative rate of phosphorescence. Such a large energy difference mainly originates from large energy splitting between HOMO ($58b_2$) and HOMO − 2 ($59b_3$) due to structural changes in the MLCT geometry.

Comparison between Two d^{10} Metal Compounds: Pt(0) and Cu(I). In this study, we found that [Pt(binap)$_2$] exhibited photophysical properties similar to those of copper(I) bis(diimine) compounds:[7] (a) delayed fluorescence at ambient temperature, (b) fairly high quantum yield of prompt fluorescence (10^{-5}−10^{-4}) with a lifetime of several picoseconds although the spin−orbit coupling constants of d electrons in the central metal are very large, and (c) fluorescence with a large Stokes shift of ca. 5.5 $\times$ 10^3 cm^{-1}.

The quantum yield of the prompt fluorescence (1.56 $\times$ 10^{-4}) of [Pt(binap)$_2$] is five times higher than that (2.8 $\times$ 10^{-5}) of $[Cu(dmp)_2]^+$ although the lifetime of the former compound is four times shorter than the latter. The higher quantum yield is caused by the observation that (a) the oscillator strength (0.21) (Table 3) of [Pt(binap)$_2$] at the lowest ^{1}MLCT state (1^1B_3) is about four times higher than that of $[Cu(dmp)_2]^+$ (0.041)[7] (1^1B_1) and (b) the formation yield of the lowest ^{1}MLCT of the platinum(0) compound upon 400 nm excitation is near unity whereas that of the copper(I) compound is estimated to be ca. 0.1. Such a small formation yield in the Cu(I) compound is probably due to the presence of a higher-lying ^{1}MLCT with an oscillator strength much stronger than that of the lowest ^{1}MLCT. The excitation of the Cu(I) compound is likely to produce a Franck−Condon state with the electron configuration of the higher-lying ^{1}MLCT, which has strong spin−orbit interaction with ^{3}MLCT so that very fast ISC may occur in competition with electronic and structural relaxation. In the Pt(0) compound, the lowest ^{1}MLCT has the highest oscillator strength and therefore possesses very low ISC opportunity during relaxation of the Franck−Condon state.

From eq 4, the equation for the quantum yield of delayed fluorescence is shown:

$$\Phi_{em,delayed} = \frac{k_{1r}K}{1+K}\tau_L \quad (9)$$

Using the k_{1r} and the ΔE values determined above, the quantum yield of delayed fluorescence was calculated to be 0.10 at 298 K. It is noteworthy that the majority of the intense emission of the Pt(0) compound in toluene at ambient temperature is delayed fluorescence from ^{1}MLCT. This interesting feature is ascribed to the following three factors: (a) the lowest ^{1}MLCT (1^1B_3) possesses a large oscillator strength yielding a radiative rate of fluorescence (4.9 $\times$ 10^7 s^{-1}), (b) the energy splitting between ^{1}MLCT and ^{3}MLCT is small (1.2 $\times$ 10^3 cm^{-1}), and (c) the lifetime of ^{3}MLCT is long (1.2 μs).

The transition dipole moment between 1^1B_3 and GS is shown approximately by the following equation:

$$M_{GS\rightarrow 1^1B_3} \propto \langle \Phi_{58b_2} | x | \Phi_{59b_1} \rangle \quad (10)$$

Putting the coefficients of the atomic orbitals in $58b_2$ and $59b_1$ and the x-positions of the atoms into eq 10, we found that the largest contribution (80%) to the integral in eq 10 comes from 2p orbitals on the naphthyl carbons. Although the contribution of the 2p orbitals on the binaphthyl moieties in $58b_2$(HOMO) is very small as shown in Figure 7, the coefficients of these 2p orbitals in $59b_1$(LUMO) are very large. In addition, a long binaphthyl−binaphthyl distance of ca. 1 nm greatly enhances the transition moment integral. Thus, the large oscillator strength of 1^1B_3 is ascribed to the π electrons on the binaphthyl moieties interacting through the platinum atom.

Energy splitting between the singlet and triplet states of the same electronic configuration is caused by the electron exchange integral, which is proportional to the spatial overlap between the MOs containing unpaired electrons.[49] In the Pt(0) compound, the HOMO is largely localized on the Pt−P σ-bonds while the LUMO is spread over binaphthyl moieties as shown in Figure 7. Thus, the spatial overlap is very small and is responsible for the smaller energy splitting between ^{1}MLCT and ^{3}MLCT in the Pt(0) compound.

Nonradiative Deactivation Pathways. The temperature dependence of nonradiative rates on the long-lived component, $(1 - \Phi_{em})\tau_L^{-1}$, shown in Figure 10 seems to be represented using an Arrhenius-type rate term and a nonactivation rate term as eq 11.

$$k_{nr}(T) = k_{nr1}\exp(-E_a/kT) + k_{nr2} \quad (11)$$

The least-squares analysis provided a pre-exponential factor (k_{nr1}) of 2.1 $\times$ 10^8 s^{-1} and activation energy (E_a) of 1.05 $\times$ 10^3 cm^{-1} in the first term and 1.2 $\times$ 10^5 s^{-1} for the value of

(49) Turro, N. J. *Modern Molecular Photochemistry*; The Benjamin/Cummings Publishing Company, Inc.,: Reading, MA, 1978.

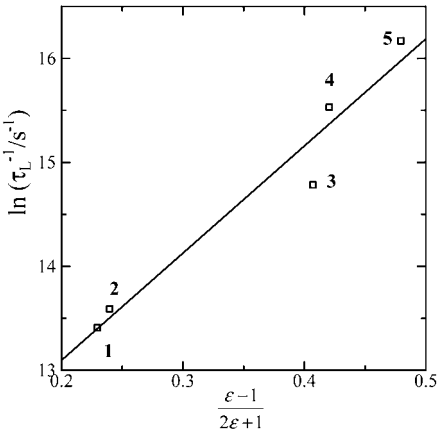

Figure 11. Plot of τ_L^{-1} as a function of a solvent polarity: (1) benzene, (2) toluene, (3) tetrahydrofuran, (4) CH_2Cl_2, (5) acetonitrile.

k_{nr2} (the broken line in Figure 10). Furthermore, the solvent dependence of the $\tau_L$values can be interpreted in terms of dipolar solvation for the transition state involved in the deactivation process. The solvation energy (E_s) for the spherical molecule having a dipole moment of μ is given by eq 11[50]

$$E_s = \frac{\mu^2}{r^3}\left(\frac{\epsilon - 1}{2\epsilon + 1}\right) \tag{11}$$

where r is the radius and ϵ is the permittivity of the solvent. The plot of the logarithm of τ_L^{-1} versus $\epsilon - 1/(2\epsilon + 1)$ shows a good relationship as seen in Figure 11, indicating that the thermal barrier in the deactivation process decreases with increasing solvent polarity. Such large solvent effects in the lifetime of ^{3}MLCT, however, seem to be inconsistent with the photophysical properties shown in Table 1. The peak energy of the steady-state emission is only weakly dependent on the solvent. In addition, the radiative rate, $\Phi_{em}\tau_L^{-1}$, which is expected to be sensitive to the energy gap between ^{1}MLCT and ^{3}MLCT at an ambient temperature, is almost unchanged between toluene and acetonitrile. Consequently, the nonradiative deactivation of the ^{3}MLCT of the Pt(0) compound probably occurs via another ^{3}MLCT of a shorter lifetime and with a dipolar electronic structure. For example, localization of the excited electron on a binap increases the dipole moment at ^{3}MLCT and thus interacts with the solvent through dipole−dipole interaction. The strong solute−solvent interaction also increases the solvent reorganization energy of the deactivation process, thereby increasing the decay rate. The observed activation energy of 1.05×10^3 cm^{-1} probably corresponds to the energy difference between the lowest nondipolar ^{3}MLCT and the higher-lying dipolar ^{3}MLCT, and the k_{nr1} of 2.1×10^8 s^{-1} is the decay rate of the ^{3}MLCT in toluene. The localization of the excited electron on one binap also causes the lowering of the coordination structure from D_2 to C_2: the shortening of the bond distance between Pt and the reduced binap, which increases the bond distance between Pt and neutral binap due to the *trans* effect.

(50) Kirkwood, J. G.; Westheimer, F. H. J. *Chem. Phys.* **1938**, *6*, 506.

Conclusion

Multiemissions of [Pt(binap)$_2$] were observed. The short-lived emission component with a quantum yield of 1.6×10^{-4} and the lifetime of 3.2 ps was assigned to prompt fluorescence from ^{1}MLCT. The long-lived emission with a quantum yield of 0.12 at 298 K was mostly due to delayed fluorescence with the peak at 13.1×10^3 cm^{-1}, which was replaced by phosphorescence with the peak at 12.0×10^3 cm^{-1} at lower temperatures.

DFT calculations of the Pt(0) compound revealed that the difference in orbital energy between HOMO and HOMO − 1 with large 5d-orbital contributions was 4.6×10^3 cm^{-1} and such a large energy splitting prevented the ISC from strong spin−orbit interaction between HOMO and HOMO − 1 (844 cm^{-1}). Thus, the ISC was induced by weak spin−orbit interaction (less than 50 cm^{-1}) between ligand-centered orbitals with very small 5d-orbital parentage. Large energy splitting in HOMOs also reduced the radiative rate of the phosphorescence. The origin of the intense MLCT band and the intense MLCT fluorescence of [Pt(binap)$_2$] was due to the high oscillator strength produced by the two binaphthyl moieties interacting through the platinum atom.

The peculiar photophysical properties of the Pt(0) compound were well rationalized by theoretical analysis, indicating that current DFT provides accurate electronic structure as well as geometry even for compounds containing heavy metal ions. Although only a few ISC rates in MLCT states have been determined so far, the relative magnitude of k_{ISC} seems to be well correlated with the square of the spin−orbit integral of the possible ISC channels. For further understanding of the factors affecting the ISC rates in MLCT states, more experimental data for various transition metal compounds are required.

Acknowledgment. Z.A.S. is thankful to the Japanese Ministry of Education, Science, Sports and Culture (Monbusho) for a graduate scholarship to pursue this research work. K.N. gratefully acknowledges financial support from Monbusho for a Grant-in-Aid for Scientific Research (14540515 and 13128206).

IC034527Z